

On Yang–Mills fields from anti-de Sitter spaces

Kaushlendra Kumar

Institute of Physics, Humboldt University, Zum Großen Windkanal 2, 12489 Berlin

E-mail: kaushlendra.kumar@hu-berlin.de

Abstract. Motivated by some recent progress involving a non-compact gauge group, we obtain classical gauge fields using non-compact foliations of anti-de Sitter space in 4 dimensions (required dimensionality for conformal invariance of Yang–Mills theory) and transfer these to Minkowski spacetime using a series of conformal maps. This construction also builds upon some previous works involving $SU(2)$ gauge group in that we now use its non-compact counterpart $SU(1,1)$ here. We note down gauge fields in both Abelian as well as non-Abelian settings and find them to be divergent at some hyperboloid, which is a hypersurface of co-dimension 1 inside the conformal boundary of AdS_4 . In spite of this hurdle we find a physically relevant field configuration in the Abelian case, reproducing a known result.

1. Introduction

Vacuum Yang–Mills theory in 4 dimensions is conformally invariant—a fact that can be used to map their solutions to any conformally related spacetime¹ after obtaining them on a more suitable one equipped with symmetric-foliations, and therefore admitting a natural gauge group. This exercise was carried out for dS_4 whose foliation submanifold S^3 arises as group manifold of $SU(2)$; the resulting $SU(2)$ -equivariant connection ansatz reproduced [4] a well known Yang–Mills solutions obtained in 1977 by Lüscher [8]. This was achieved by following set of conformal correspondences: $\mathcal{I} \times S^3 \xleftarrow{\text{conformal}} dS_4 \xrightarrow{\text{conformal}} \mathbb{R}^{1,3}$ where the cylinder domain $\mathcal{I} = (-\frac{\pi}{2}, \frac{\pi}{2})$ needs to be doubled to facilitate a gluing of two dS_4 copies so as to cover entire Minkowski spacetime. Furthermore, solutions for its Abelian counterpart $U(1) \subset SU(2)$ (in a non-symmetric setting) produces a family of electromagnetic knotted fields [4, 5]. These EM knots have rather intriguing physical features, many of which have been explored recently [6, 7]. Another motivation for such an exploration of classical gauge fields is that only a few of them are known in mathematical physics literature (see e.g. [1, 2, 3] for reviews). To this end, novel results were obtained on de Sitter and anti-de Sitter spaces in [10, 11] for $SU(2)$ as well as some higher-dimensional generalizations (in de Sitter case) for $SO(4)$ in [12].

There has been some recent progress [13] towards obtaining gauge fields via H^3 and dS_3 foliations of Minkowski space regions with non-compact gauge group $SO(1,3)$, as opposed to compact ones discussed above. Inspired by this success, we considered AdS_3 foliations of AdS_4 since the former arises as group manifold of $SU(1,1)$. Classical gauge fields were obtained here for $SU(1,1)$ -symmetric gauge configuration [14] (of both Abelian and non-Abelian type) by employing following strategy: $\mathcal{I} \times AdS_3 \xleftarrow{\text{conformal}} AdS_4 \xrightarrow{\text{conformal}} \mathcal{I} \times S^3_+$ followed by the

¹ It is a known fact that all three variants of FLRW spacetimes viz. Minkowski $\mathbb{R}^{1,3}$, de Sitter dS_4 and anti-de Sitter AdS_4 are covered this way.

previous $\mathcal{I} \times S^3 \xrightarrow{\text{conformal}} \mathbb{R}^{1,3}$ after gluing two AdS_4 copies to recover full S^3 . However, unlike the previous compact case, this gluing is not smooth and leads to a singular conformal boundary; this feature propagates to the corresponding gauge fields but in a milder fashion. We present such field configurations in a compact form and compute their stress energy tensor. We also make use of several plots to explain various features of these conformal maps and resulting field configurations (such as orientation preserving gluing).

2. Geometrical toolkit for anti-de Sitter space AdS_4

We start with the following isometric embedding of AdS_4 —endowed with coordinates $(x^1, x^2, x^3, x^4, x^5)$ and global radius R —inside $\mathbb{R}^{2,3}$ via

$$-(x^1)^2 - (x^2)^2 + (x^3)^2 + (x^4)^2 + (x^5)^2 = -R^2 . \quad (1)$$

2.1. AdS_4 -foliations of the form $\mathcal{I} \times \mathcal{M}_3$

First, we have $\mathcal{M}_3 = \text{AdS}_3$ foliation with a spacelike parameter $\psi \in \mathcal{I} = (-\pi/2, \pi/2)$. This $\text{AdS}_3 \hookrightarrow \mathbb{R}^{2,2}$ can be described using embedding coordinates $\alpha^i(\rho, \tau, \phi)$ for $i = 1, \dots, 4$ with spatial parameters $\rho \in \mathbb{R}_+$, $\phi \in [0, 2\pi]$ and temporal parameter $\tau \in [0, 2\pi]$ as

$$\begin{aligned} \alpha^1 &= \cosh \rho \cos \tau, & \alpha^2 &= \cosh \rho \sin \tau, \\ \alpha^3 &= \sinh \rho \cos \phi, & \alpha^4 &= \sinh \rho \sin \phi, \end{aligned} \quad \implies \quad -(\alpha^1)^2 - (\alpha^2)^2 + (\alpha^3)^2 + (\alpha^4)^2 = -1 . \quad (2)$$

The following global AdS_4 embedding coordinates,

$$x^i = R \sec \chi \alpha^i, \quad x^5 = R \tan \chi , \quad (3)$$

then yields its induced metric (arising from flat $\mathbb{R}^{2,3}$ metric) in terms of AdS_3 metric $d\Omega_{1,2}^2$ as

$$ds^2 = \frac{R^2}{\cos^2 \psi} (d\psi^2 - \cosh^2 \rho d\tau^2 + d\rho^2 + \sinh^2 \rho d\phi^2) = \frac{R^2}{\cos^2 \psi} (d\psi^2 + d\Omega_{1,2}^2) . \quad (4)$$

Next, we have $\mathcal{M}_3 = S_+^3$ (upper hemisphere) foliations, embedded inside $\mathbb{R}^{2,3}$ using

$$x^1 = R \sec \chi \cos \tau, \quad x^2 = R \sec \chi \sin \tau, \quad x^3 = R \tan \chi \beta^1, \quad x^4 = R \tan \chi \beta^2, \quad x^5 = R \tan \chi \beta^3 , \quad (5)$$

where $\chi \in [0, \pi/2)$ for the half-sphere and canonical S^2 coordinates $\beta^i(\theta, \phi)$ with $\theta \in [0, \pi]$ are

$$\beta^1 = \sin \theta \cos \phi, \quad \beta^2 = \sin \theta \sin \phi, \quad \beta^3 = \cos \theta . \quad (6)$$

These are related to the coordinates (ρ, ψ) above (3) as follows,

$$\tanh \rho = \sin \theta \sin \chi \quad \text{and} \quad \tan \psi = -\cos \theta \tan \chi . \quad (7)$$

In this case, the induced metric demonstrates a S_+^3 -cylinder structure with round metric $d\Omega_{3+}^2$; the latter can be expressed using S^2 round metric $d\Omega_2^2$ as

$$ds^2 = \frac{R^2}{\cos^2 \chi} (-d\tau^2 + d\chi^2 + \sin^2 \chi d\Omega_2^2) = \frac{R^2}{\cos^2 \chi} (-d\tau^2 + d\Omega_{3+}^2) . \quad (8)$$

This temporal parameter τ can be extended to full \mathbb{R} by going to the universal cover $\widetilde{\text{AdS}}_4$.

Table 1. Key points on northern hemisphere ($\varepsilon = +1; P$) and southern hemisphere ($\varepsilon = -1; P'$) in two coordinate systems for some infinitesimal $\epsilon > 0$.

S_+^3	$(\rho, \psi)_+$	$(\chi, \theta)_-$	S_-^3	$(\rho, \psi)_-$	$(\chi, \theta)_-$
P_1	$(0, 0 - \epsilon)$	$(0, 0)$	P'_1	$(0, 0 - \epsilon)$	$(\pi, 0)$
P_2	$(0, -\frac{\pi}{2})$	$(\frac{\pi}{2}, 0)$	P'_2	$(0, -\frac{\pi}{2})$	$(\frac{\pi}{2}, 0)$
P_3	$(\infty, -\frac{\pi}{2})$	$(\frac{\pi}{2}, \frac{\pi}{2} - \epsilon)$	P'_3	$(-\infty, -\frac{\pi}{2})$	$(\frac{\pi}{2}, \frac{\pi}{2} - \epsilon)$
P_4	$(\infty, \frac{\pi}{2})$	$(\frac{\pi}{2}, \frac{\pi}{2} + \epsilon)$	P'_4	$(-\infty, \frac{\pi}{2})$	$(\frac{\pi}{2}, \frac{\pi}{2} + \epsilon)$
P_5	$(0, \frac{\pi}{2})$	$(\frac{\pi}{2}, \pi)$	P'_5	$(0, \frac{\pi}{2})$	$(\frac{\pi}{2}, \pi)$
P_6	$(0, 0 + \epsilon)$	$(0, \pi)$	P'_6	$(0, 0 + \epsilon)$	(π, π)

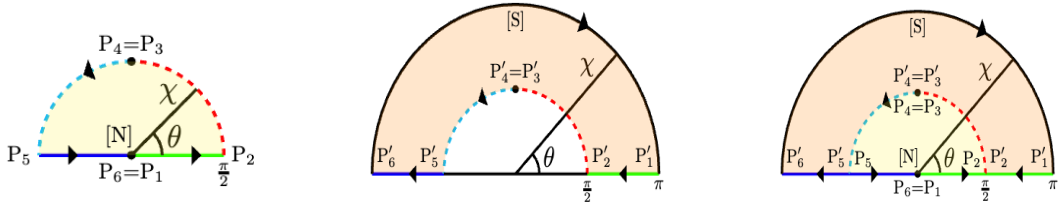


Figure 1. Depiction of S_+^3 -boundary with colored segments between key points.

Figure 2. Depiction of S_-^3 -boundary with colored segments between key points.

Figure 3. Depiction of the gluing across S^2 boundary while preserving orientation.

2.2. Gluing of two AdS₄ copies

We now proceed to glue two copies of AdS₄ to recover full round 3-sphere, i.e. $S^3 = S_+^3 \cup S^2 \cup S_-^3$ in order to apply below-mentioned conformal map. To this end, we note down the following map that glues northern copy S_+^3 with southern one S_-^3 along the boundary S^2 at $\chi = \frac{\pi}{2}$:

$$\begin{aligned} \tanh \rho &= \varepsilon \sin \theta \sin \chi \quad \text{and} \quad \tan \psi = -\varepsilon \cos \theta \tan \chi, \quad \text{with} \\ \varepsilon|_{S_+^3} = +1 : \rho \in \mathbb{R}_+ &\Leftrightarrow \chi \in [0, \frac{\pi}{2}) \quad \text{and} \quad \varepsilon|_{S_-^3} = -1 : \rho \in \mathbb{R}_- \Leftrightarrow \chi \in (\frac{\pi}{2}, \pi]. \end{aligned} \quad (9)$$

This map preserves the orientation along the gluing boundary $\partial S_{\pm}^3 = S^2$. To see this, we note down some key points in table 1 for both coordinate systems and then plot these in spherical coordinates $(\chi, \theta)^2$ individually in figures 1 and 2 as well as in combined fashion in figure 3. Notice in the figures that the open boundary of the AdS space (for fixed τ) is depicted with dashed lines while some points (like the north pole) are identified as is clear from table 1. Finally, the gluing happens by identifying the points (P_2, \dots, P_5) with (P'_2, \dots, P'_5) pairwise so that same-colored segments are coincide and the orientation remains preserved. Another point to note here is that this gluing is not smooth, but consists of a singularity arising from the conformal boundary $\chi = \pi/2$ as is clear from above metric (8).

2.3. Conformal mapping to Minkowski space $\mathbb{R}^{1,3}$

So far, we have seen an effective conformal map between AdS₃-cylinder (4) and S^3 -cylinder (8,9): $(\rho, \psi) \rightarrow (\chi, \theta)$ while keeping τ and ϕ fixed. We can now map the S^3 -cylinder (post-

² This could also be demonstrated in other coordinate system as well; see [14] for details.

gluing) to Minkowski space $\mathbb{R}^{1,3}$ equipped with polar coordinates (t, r, θ, ϕ) ³: $(\tau, \chi) \rightarrow (t, r)$ via

$$\sin \tau = \gamma \frac{t}{R} \quad \text{and} \quad \sin \chi = \gamma \frac{r}{R} \quad \text{with} \quad \gamma = \frac{2R^2}{\sqrt{4R^2t^2 + (r^2 - t^2 + R^2)^2}}, \quad (10)$$

where the S^2 coordinates (θ, ϕ) are identified. A key feature of this map is that the full Minkowski space gets embedded inside half of the doubled AdS domain with null-boundary given by $\chi=|\tau|$; this is due to the following inequality:

$$\gamma = \cos \tau - \cos \chi > 0 \quad \implies \quad \chi > |\tau|. \quad (11)$$

This feature is clearly exemplified through (τ, χ) Penrose diagram in figure 4 demonstrating the flat spacetime embedding inside half of the (glued) AdS₄ space with future and past null boundaries. The (t, r) plot in figure 5 further illustrates the gluing-boundary inside Minkowski spacetime. It should be noted here that every point inside shaded regions of these plots hides a 2-sphere and that such regions coming from different AdS₄ copies are color-coded (yellow and orange shades).

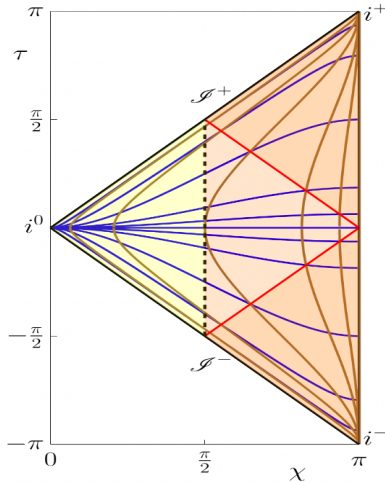


Figure 4. Penrose diagram inside AdS₄ spaces joined together (dotted black line) with constant (blue lines) t - and (brown lines) r -hypersurfaces and the lightcone at the origin (red lines).

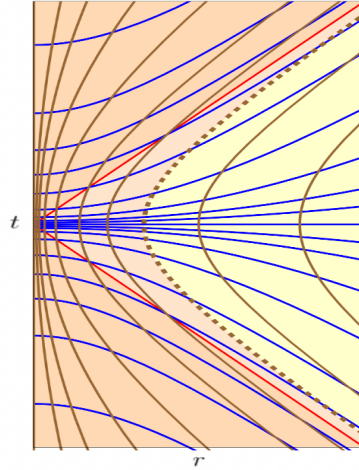


Figure 5. Minkowski spacetime in polar coordinates (t, r) with constant τ - & χ -slices shown in blue and brown lines respectively while the broken brown line shows the gluing-boundary.

The conformal metric (8) in these Minkowski coordinates take the following form:

$$ds^2 = \frac{4R^4}{(r^2 - t^2 - R^2)^2} (-dt^2 + dr^2 + r^2 d\Omega_2^2), \quad (12)$$

which shows that the singularity at the gluing-boundary is a one-sheeted hyperboloid $H_R^{1,2}$:

$$\{\chi = \frac{\pi}{2}\} \quad \iff \quad \{r^2 - t^2 = R^2\} =: H_R^{1,2}. \quad (13)$$

³ Let us recall Minkowski polar coordinates: $(t, x, y, z) = (t, r \sin \theta \cos \phi, r \sin \theta \sin \phi, r \cos \theta)$.

3. SU(1, 1)-symmetric gauge theory on AdS₄

Let us review some algebraic results required to construct the relevant connection one-form. To this end, we start with the group manifold of SU(1, 1) which is AdS₃, easily seen by the map

$$g : \text{AdS}_3 \rightarrow \text{SU}(1, 1) \quad \text{via} \quad (\alpha^1, \alpha^2, \alpha^3, \alpha^4) \mapsto \begin{pmatrix} \alpha^1 - i\alpha^2 & \alpha^3 - i\alpha^4 \\ \alpha^3 + i\alpha^4 & \alpha^1 + i\alpha^2 \end{pmatrix}. \quad (14)$$

We use this g to obtain left-invariant one-forms e^α , $\alpha = 0, 1, 2$ via Maurer–Cartan method:

$$\Omega_L(g) = g^{-1}dg = e^\alpha I_\alpha \quad (15)$$

where I_α are $\mathfrak{sl}(2, \mathbb{R})$ generators satisfying

$$[I_\alpha, I_\beta] = 2f_{\alpha\beta}^\gamma I_\gamma \quad \text{and} \quad \text{tr}(I_\alpha I_\beta) = 2\eta_{\alpha\beta}, \quad (16)$$

with $f_{01}^2 = f_{20}^1 = -f_{12}^0 = 1$ and $(\eta_{\alpha\beta}) = \text{diag}(-1, 1, 1)$. The resulting one-forms look like,

$$\begin{aligned} e^0 &= \cosh^2 \rho \, d\tau + \sinh^2 \rho \, d\phi, \\ e^1 &= \cos(\tau - \phi) \, d\rho + \sinh \rho \cosh \rho \sin(\tau - \phi) \, d(\tau + \phi), \\ e^2 &= -\sin(\tau - \phi) \, d\rho + \sinh \rho \cosh \rho \cos(\tau - \phi) \, d(\tau + \phi). \end{aligned} \quad (17)$$

These obey Cartan structure equation and provide orthonormal-frame on AdS₃-cylinder (4):

$$de^\alpha + f_{\beta\gamma}^\alpha e^\beta \wedge e^\gamma = 0 \quad \text{and} \quad ds_{\text{cyl}}^2 = d\psi^2 + \eta_{\alpha\beta} e^\alpha e^\beta. \quad (18)$$

Now a generic *gauge field* \mathcal{A} in this frame can be made SU(1, 1)-symmetric by,

$$\begin{aligned} \mathcal{A} &= \mathcal{A}_\psi e^\psi + \mathcal{A}_\alpha e^\alpha \quad \xrightarrow{\mathcal{A}_\psi=0} \quad \mathcal{A} = X_\alpha(\psi) e^\alpha \\ \implies \mathcal{F} &= d\mathcal{A} + \mathcal{A} \wedge \mathcal{A} = X'_\alpha e^\psi \wedge e^\alpha + \frac{1}{2}(-2f_{\beta\gamma}^\alpha X_\alpha + [X_\beta, X_\gamma]) e^\beta \wedge e^\gamma, \end{aligned} \quad (19)$$

where X'_α in the field strength expression correspond to $dX_\alpha/d\psi$. Next, we impose the Gauss-law constraint $[X_\alpha, X'_\alpha] = 0$ arising from the eom $*d*\mathcal{F} = 0$ by following choice of components,

$$X_0 = \Theta_0(\psi) I_0, \quad X_1 = \Theta_1(\psi) I_1 \quad \text{and} \quad X_2 = \Theta_2(\psi) I_2. \quad (20)$$

The Yang–Mills Lagrangian $\mathcal{L} = \frac{1}{4} \text{tr}(\mathcal{F} \wedge *\mathcal{F})$ can then be readily computed to get,

$$\begin{aligned} \mathcal{L} &= \frac{1}{4} \text{tr} \mathcal{F}_{\psi\alpha} \mathcal{F}^{\psi\alpha} + \frac{1}{8} \text{tr} \mathcal{F}_{\beta\gamma} \mathcal{F}^{\beta\gamma} \\ &= \frac{1}{2} \sum_\alpha (\Theta'_\alpha)^2 - 2\{(\Theta_1 - \Theta_2 \Theta_0)^2 + (\Theta_2 - \Theta_0 \Theta_1)^2 + (\Theta_0 - \Theta_1 \Theta_2)^2\}. \end{aligned} \quad (21)$$

This enjoys discrete symmetry of the permutation group S_4 , acting by permuting $\{\Theta_\alpha\}$ and flipping the sign of any two Θ' s. Its maximal normal subgroups S_3 and D_8 yields *exact solutions*:

- **Non-equivariant Abelian ansätze:**

$$\Theta_0 \text{ or } \Theta_1 \text{ or } \Theta_2 = h(\psi) \quad \text{while} \quad \text{rest} = 0 \quad \implies \quad h'' = -4h, \quad (22)$$

resulting into a harmonic equation whose solutions are well-known trigonometric functions.

- **Equivariant non-Abelian ansatz:**

$$\Theta_0 = \Theta_1 = \Theta_2 =: \frac{1}{2}(1 + \Phi(\psi)) \quad \implies \quad \Phi'' = 2\Phi(1 - \Phi^2) = -\frac{\partial V}{\partial \Phi}, \quad (23)$$

where the double-well potential $V(\Phi) = \frac{1}{2}(\Phi^2 - 1)^2$ has been plotted in figure 6. The resultant anharmonic equation here also admits analytic solutions in terms of Jacobi elliptic functions.

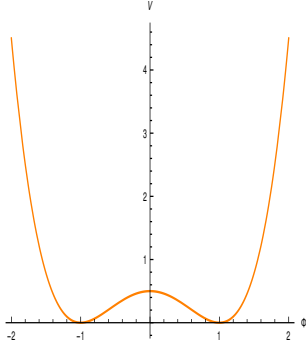


Figure 6. Plot of the potential $V(\Phi)$.

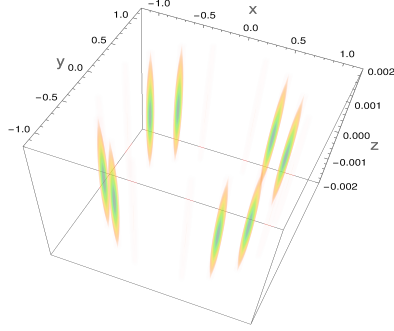


Figure 7. Color-graded density plot for the energy density $\rho \propto \frac{1}{(\lambda^2+4z^2)^2}|_{t=0}$ emphasizing its maxima near $z=0$.

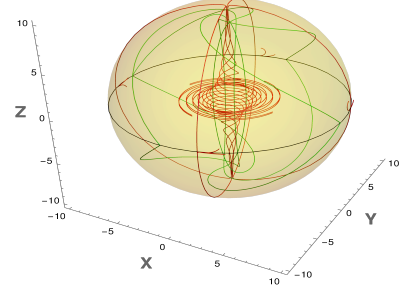


Figure 8. Electric (red) and magnetic (green) field lines for $\tilde{\mathbf{S}}^{(0)}$ at $t=10$ and $\psi_0=\frac{\pi}{2}$ inside the sphere of radius $r=\sqrt{101}$.

4. AdS₄ gauge fields on Minkowski space

We have already seen a series of conformal maps $(\tau, \rho, \psi) \rightarrow (\tau, \chi, \theta) \rightarrow (t, r, \theta)$ defined via (9) and (10) above. We can use these with $R=1$ along with abbreviations $x \cdot dx := x_\mu dx^\mu$, $\varepsilon^1 = \varepsilon^2 := \varepsilon$ and $\varepsilon^0 := 1$ to write the AdS₃-cylinder one-forms e^α (17) and $e^\psi := d\psi$ in Minkowski coordinates as,

$$\begin{aligned} e^\alpha &= \frac{\varepsilon^\alpha}{\lambda^2+4z^2} \left(2(\lambda+2) dx^\alpha - 4x^\alpha x \cdot dx - 4 f_{\beta\gamma}^\alpha x^\beta dx^\gamma \right), \\ e^\psi &= \frac{\varepsilon}{\lambda^2+4z^2} \left(-2\lambda dz + 4z x \cdot dx \right), \quad \text{where } \lambda := r^2 - t^2 - 1. \end{aligned} \quad (24)$$

This allows one to read-off various vierbein components, viz. e_μ^α and e_μ^ψ to be used below.

4.1. Nonabelian fields

For the nonabelian case we use the the ansatz (23) for gauge field \mathcal{A} (19). The corresponding field strength F of $\mathcal{A} \equiv A = \frac{1}{2} \left(1 + \Phi(\psi(x)) \right) I_\alpha e_\mu^\alpha dx^\mu$ then computes to,

$$F = \frac{1}{2} \left(\Phi'(\psi(x)) I_\alpha e_\mu^\psi e_\nu^\alpha - \frac{1}{2} (1 - \Phi(\psi(x)))^2 I_\alpha f_{\beta\gamma}^\alpha e_\mu^\beta e_\nu^\gamma \right) dx^\mu \wedge dx^\nu. \quad (25)$$

One can easily extract the color-electromagnetic fields from this F as follows: $E_a := F_{a0}$ and $B_a := \frac{1}{2} \epsilon_{abc} F_{bc}$. We can express the color EM fields thus obtained rather succinctly in terms of a Riemann–Silberstein vector $\mathbf{S} := \mathbf{E} + i\mathbf{B}$ as,

$$S_x = -\frac{2(i\varepsilon\Phi'+\Phi^2-1)}{(\lambda-2iz)(\lambda+2iz)^2} \left\{ 2[ty+ix(z+i)]I_0 + 2\varepsilon[xy+it(z+i)]I_1 + \varepsilon[t^2-x^2+y^2+(z+i)^2]I_2 \right\}, \quad (26)$$

$$S_y = \frac{2(i\varepsilon\Phi'+\Phi^2-1)}{(\lambda-2iz)(\lambda+2iz)^2} \left\{ 2[tx-iy(z+i)]I_0 + \varepsilon[t^2+x^2-y^2+(z+i)^2]I_1 + 2\varepsilon[xy-it(z+i)]I_2 \right\}, \quad (27)$$

$$S_z = \frac{2(i\varepsilon\Phi'+\Phi^2-1)}{(\lambda-2iz)(\lambda+2iz)^2} \left\{ i[t^2+x^2+y^2-(z+i)^2]I_0 + 2\varepsilon[itx-y(z+i)]I_1 + 2\varepsilon[ity+x(z+i)]I_2 \right\}. \quad (28)$$

Interestingly, any explicit solution Φ do not couple to color components of these fields \mathbf{S} ; this fact reflects below in that the corresponding physical quantities (arising from the stress-energy tensor) depends only on a conserved parameter—rather than an explicit form—of such solutions.

We can now compute the corresponding stress-energy tensor $T_{\mu\nu}$ given by,

$$T_{\mu\nu} = -\frac{1}{2g^2} (\delta_\mu^\rho \delta_\nu^\lambda \eta^{\sigma\tau} - \frac{1}{4} \eta_{\mu\nu} \eta^{\rho\lambda} \eta^{\sigma\tau}) \text{tr}(F_{\rho\sigma} F_{\lambda\tau}) , \quad (29)$$

and express them, using mechanical energy $\epsilon := -\frac{1}{4}((\Phi')^2 + (1-\Phi^2)^2)$, compactly as follows:

$$(T_{\mu\nu}) = \frac{8}{g^2} \frac{\epsilon}{(\lambda^2+4z^2)^3} \begin{pmatrix} \mathbf{t}_{\alpha\beta} & \mathbf{t}_{\alpha 3} \\ \mathbf{t}_{3\alpha} & \mathbf{t}_{33} \end{pmatrix} \quad \text{with} \quad \begin{cases} \mathbf{t}_{\alpha\beta} = -\eta_{\alpha\beta}(\lambda^2+4z^2) + 16x_\alpha x_\beta z^2 , \\ \mathbf{t}_{3\alpha} = \mathbf{t}_{\alpha 3} = -8x_\alpha z(\lambda-3z^2) , \\ \mathbf{t}_{33} = 3\lambda^2 - 4z^2(1+4\lambda-4z^2) . \end{cases} \quad (30)$$

We find that these fields \mathbf{E}, \mathbf{B} and their stress-energy tensor $T_{\mu\nu}$ are not singular at the full hyperboloid $H^{1,2} \equiv \lambda=0$ but on a hypersurface given by the intersection

$$\{\lambda=0\} \cap \{z=0\} \Leftrightarrow x^2 + y^2 - t^2 = 1 . \quad (31)$$

We have plotted the energy density $\rho = \mathbf{t}_{00}$ at $t=0$ highlighting the role of xy -plane in figure 7.

4.2. Electromagnetic fields

We consider following harmonic functions as solutions to the Abelian eom (22) such that they would have same structural form across the gluing surface (mediated by ε):

$$\begin{aligned} \tilde{A}^{(0)} &= -\frac{1}{2} \cos 2(\psi(x)+\varepsilon\psi_0) e^0_\mu dx^\mu , \\ \tilde{A}^{(1)} &= \frac{1}{2} \sin 2(\psi(x)+\varepsilon\psi_0) e^1_\mu dx^\mu , \\ \tilde{A}^{(2)} &= \frac{1}{2} \sin 2(\psi(x)+\varepsilon\psi_0) e^2_\mu dx^\mu . \end{aligned} \quad (32)$$

As before, we can go ahead and compute the corresponding field strengths \tilde{F} , e.g. this one

$$\tilde{F}^{(0)} = \{ \sin 2(\psi(x)+\varepsilon\psi_0) e^\psi_\mu e^0_\nu - \cos 2(\psi(x)+\varepsilon\psi_0) e^1_\mu e^2_\nu \} dx^\mu \wedge dx^\nu , \quad (33)$$

and then extract the electric $\tilde{\mathbf{E}}$ and magnetic $\tilde{\mathbf{B}}$ fields. These can again be casted into a nice compact form using Riemann–Silberstein vector $\tilde{\mathbf{S}} := \tilde{\mathbf{E}} + i\tilde{\mathbf{B}}$ as follows,

$$\tilde{\mathbf{S}}^{(0)} = \frac{4e^{2i\psi_0}}{(\lambda+2iz)^3} \begin{pmatrix} -2(ty + ix(z+i)) \\ 2(tx - iy(z+i)) \\ i(t^2 + x^2 + y^2 - (z+i)^2) \end{pmatrix} , \quad (34)$$

$$\tilde{\mathbf{S}}^{(1)} = -\frac{4e^{2i\psi_0}}{(\lambda+2iz)^3} \begin{pmatrix} 2i(xy + it(z+i)) \\ -i(t^2 + x^2 - y^2 + (z+i)^2) \\ 2(tx + iy(z+i)) \end{pmatrix} , \quad (35)$$

$$\tilde{\mathbf{S}}^{(2)} = \frac{4e^{2i\psi_0}}{(\lambda+2iz)^3} \begin{pmatrix} -i(t^2 - x^2 + y^2 + (z+i)^2) \\ 2i(xy - it(z+i)) \\ -2(ty - ix(z+i)) \end{pmatrix} . \quad (36)$$

Like before, these fields are also singular on the hypersurface (31). We demonstrate this in figure 8 by plotting typical field lines for $\tilde{\mathbf{E}}^{(0)}$ and $\tilde{\mathbf{B}}^{(0)}$ (34); these accumulate and intersect at the singular boundary (denoted with black circle). We omit here the expressions for the

stress-energy components (due to their bulky form) and refer the reader to [14], where such expressions corresponding to fields in (34) have been noted.

Incidentally, the above Riemann–Silberstein vectors are reminiscent of the Hopf–Rañada (HR) electromagnetic knots [4] and suggests their interpretation as a non-compact cousin of the HR knot. Upon further exploration we find that a special case of the field configuration (34):

$$\psi_0 = z = 0 \quad \Longrightarrow \quad \frac{4}{(x^2+y^2-t^2-1)^3} \begin{pmatrix} 2(x-ty) \\ 2(y+tx) \\ t^2+x^2+y^2+1 \end{pmatrix}, \quad (37)$$

reproduces the magnetic fields⁴ of a recently constructed magnetic vortex [15, eq. (5.15)] under the following identification of the AdS₃ coordinates (x^0, x^1, x^2) used in [15],

$$x^0 = -t, \quad x^1 = -y \quad \text{and} \quad x^2 = x. \quad (38)$$

5. Summary

- First, we employed the AdS₃-slicing of AdS₄ and the group manifold structure of SU(1, 1) to find Yang–Mills solutions on $\mathcal{I} \times \text{AdS}_3$.
- Next, we used a series of conformal maps to transfer these solutions to Minkowski space, since Yang–Mills theory is conformally invariant in 4-dimensions.
- These gauge fields are singular on a 2-dimensional hyperboloid $x^2+y^2-t^2 = 1$, but this singularity is milder than the one we started with, namely $r^2-t^2-1 = 0$.
- Due to this singularity the total energy diverges for both kinds of gauge fields (see [14] for details), thereby limiting their physical usefulness.
- Nevertheless, our Abelian solutions were found to match the magnetic field of a known vortex magnetic mode on SU(1, 1) [15]. The status of other two Abelian solutions in this regard remains to be explored.

References

- [1] Actor A 1979 *Rev. Mod. Phys.* **51** 461
- [2] Rajaraman R 1984 *Solitons and instantons* (Amsterdam: North-Holland)
- [3] Manton N and Sutcliffe P 2004 *Topological solitons* (Cambridge: Cambridge University Press)
- [4] Lechtenfeld O and Zhilin G 2018 *Phys. Lett. A* **382** 1528 (*Preprint* 1711.11144)
- [5] Kumar K and Lechtenfeld O 2020 *Phys. Lett. A* **384** 126445 (*Preprint* 2002.01005)
- [6] Hantzko L, Kumar K and Picanço Costa G 2022 *Eur. Phys. J. Plus* **137** 407 (*Preprint* 2106.05952)
- [7] Kumar K, Lechtenfeld O and Picanço Costa G 2022 *J. Phys. A: Math. Theor.* **55** 315401 (*Preprint* 2202.00169)
- [8] Lüscher M 1977 *Phys. Lett.* **70B** 321
- [9] Arrayás M, Bouwmeester D and Trueba J L 2017 *Phys. Rept.* **667** 1
- [10] Ivanova T A, Lechtenfeld O and Popov A D 2017 *Phys. Rev. Lett.* **119** 061601 (*Preprint* 1704.07456)
- [11] Ivanova T A, Lechtenfeld O and Popov A D 2017 *J. High Energy Phys.* JHEP11(2017)017 (*Preprint* 1708.06361)
- [12] Lechtenfeld O and Ünal G 2018 *Phys. Rev. D* **98** 085008 (*Preprint* 1807.03914)
- [13] Kumar K, Lechtenfeld O, Picanço Costa G and Röhrig J 2022 *Phys. Lett. B* **835** 137564 (*Preprint* 2206.12009)
- [14] Hirpara S, Kumar K, Lechtenfeld O and Picanço Costa G 2023 Exact gauge fields from anti-de Sitter space *Preprint* 2301.03606
- [15] Ross C and Schroers B J 2018 *J. Phys. A: Math. Theor.* **51** 295202 (*Preprint* 1803.11120)

⁴ In our convention, these gauge fields are interpreted as two electric fields and one magnetic field.